S-Parameter De-Embedding Error Estimation Based on the Statistical Circuit Models of Fixtures

Yuanzhuo Liu, *Student Member, IEEE*, Shaohui Yong, *Student Member, IEEE*, Han Gao, *Student Member, IEEE*, Scott Hinaga, Darja Padilla, Douglas Yanagawa, James L. Drewniak, *Fellow, IEEE*, and Victor Khilkevich, *Member, IEEE*

***Abstract*—*S*-parameter de-embedding methods require multiple fixtures to be identical. However, due to manufacturing variations, the fixtures are never perfectly identical, which violates the assumptions for the de-embedding algorithms and, in turn, introduces errors. In this article, a novel methodology is proposed to estimate the errors due to de-embedding for practical transmission line measurements. The circuit models of the thru and total lines with fixtures are created. Perturbation in the fixtures is introduced based on the fixture variation estimated by time-domain reflectometry measurements. The method can predict the envelope and estimate the confidence interval of the de-embedded insertion loss using a limited number of simulation cases.**

***Index Terms*—Confidence interval, de-embedding, error analysis, fixtures, thru-reflect-line (TRL), transmission line measurements, 2X-thru.**

I. Introduction

With the evolution of high-speed electronic devices, the data rates have been raised to the level of 50 Gb/s and above. As communication speed increases, the characterization of the high-speed channels has become a critical issue. At the frequencies of tens of gigahertz, the nonideal transmission line issues (such as copper surface roughness, dielectric dispersion, and glass-weave effect) are no longer negligible and the attenuation of transmission lines needs to be measured precisely.

The transmission lines on a fabricated printed circuit board (PCB) often require test fixtures for interconnection. To remove the discontinuities introduced by the fixtures (such as connector/probe attachments, vias, and transition sections), the de-embedding procedures are applied; namely, the calibration reference planes are moved from the coaxial connectors to the PCB interfaces [1].

Different de-embedding approaches were brought up for the high-speed transmission line characterization. The prevailing de-embedding methodologies include thru-reflect-line (TRL) [2], 2X-thru [3], [4], and smart fixtures de-embedding (SFD) [5], [6]. The TRL method can cover a wideband of frequencies by measuring multiple line standards with different lengths and has become a mainstream approach. Compared with the TRL method, 2X-thru de-embedding methodology simplifies the standard design and the measurement procedure. Alternatively, the SFD commercial tool can be used to perform the same task.

Theoretically, all de-embedding methods require identical fixtures on total and thru lines. Besides, 2X-thru de-embedding needs symmetric design in fixtures for both total and thru lines. However, manufacturing variations make it challenging to implement identical or symmetrical structures. As a result, the identical assumptions are unavoidably violated, which results in a de-embedding error. Besides, inappropriate operations in measurement, such as loosely attached connectors or probes, also contribute to de-embedding error.

The de-embedding procedure is the necessary step in many transmission line characterization algorithms, for example, crosstalk analysis [7]–[9], copper foil roughness modeling [10], [11], and dielectric material property extraction [12]. As such, the de-embedding error is introduced into the characterization algorithms and may get amplified due to the nonlinear transformations afterward. Therefore, in order to estimate the accuracy of characterization, it is important to assess the accuracy of the raw data (*S*-parameters).

Sensitivity investigations for various de-embedding algorithms were presented in [13]–[16] to illustrate the impact of the nonideal fixtures. Generally, they follow the idea of establishing "perfect" *S*-parameters with identical fixtures, then introducing a perturbation factor in fixtures and rederive the de-embedding algorithm with the perturbation factor. Such an approach provides an insight into the mechanism of de-embedding error generation. However, the difficulty in defining the "perfect" *S*-parameters and the perturbation for practical measurements' limits the usage of these approaches.

In [16], another method was proposed to estimate the boundary of de-embedded results. It is based on an *a priori* assumption that the reflection coefficient S_{11} is varying within a circle on a

Manuscript received December 14, 2019; revised April 9, 2020; accepted April 23, 2020. Date of publication June 1, 2020; date of current version August 13, 2020. This work was supported by the National Science Foundation under Grant IIP-1440110. This article was presented in part at the IEEE Symposium on Electromagnetic Compatibility, Signal and Power Integrity, Singapore and New Orleans, LA, USA, July 2019. *(Corresponding author: Yuanzhuo Liu.)*

Yuanzhuo Liu, Shaohui Yong, James L. Drewniak, and Victor Khilkevich are with the Electromagnetic Compatibility Laboratory, Missouri University of Science and Technology, Rolla, MO 65401 USA (e-mail: liuyuanz@umsystem.edu; sy2m5@umsystem.edu; drewniak@umsystem.edu; khilkevichv@umsystem.edu).

Han Gao, Scott Hinaga, Darja Padilla, and Douglas Yanagawa are with the Cisco Systems, Inc., San Jose, CA 95134 USA (e-mail: hgao2@cisco.com; shinaga@cisco.com; darja@cisco.com; 7yanagawa@cisco.com).

Color versions of one or more of the figures in this article are available online at https://ieeexplore.ieee.org.

Digital Object Identifier 10.1109/TEMC.2020.2992553

0018-9375 © 2020 IEEE. Personal use is permitted, but republication/redistribution requires IEEE permission.
See https://www.ieee.org/publications/rights/index.html for more information.

Authorized licensed use limited to: Missouri University of Science and Technology. Downloaded on February 01,2021 at 01:15:11 UTC from IEEE Xplore. Restrictions apply.

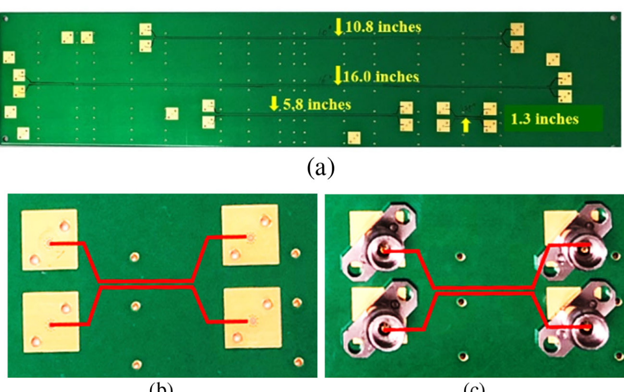

Fig. 1. (a) Testing vehicle with several coupled striplines of different lengths. Photos of the 1.3-in differential pair (b) without and (c) with connectors.

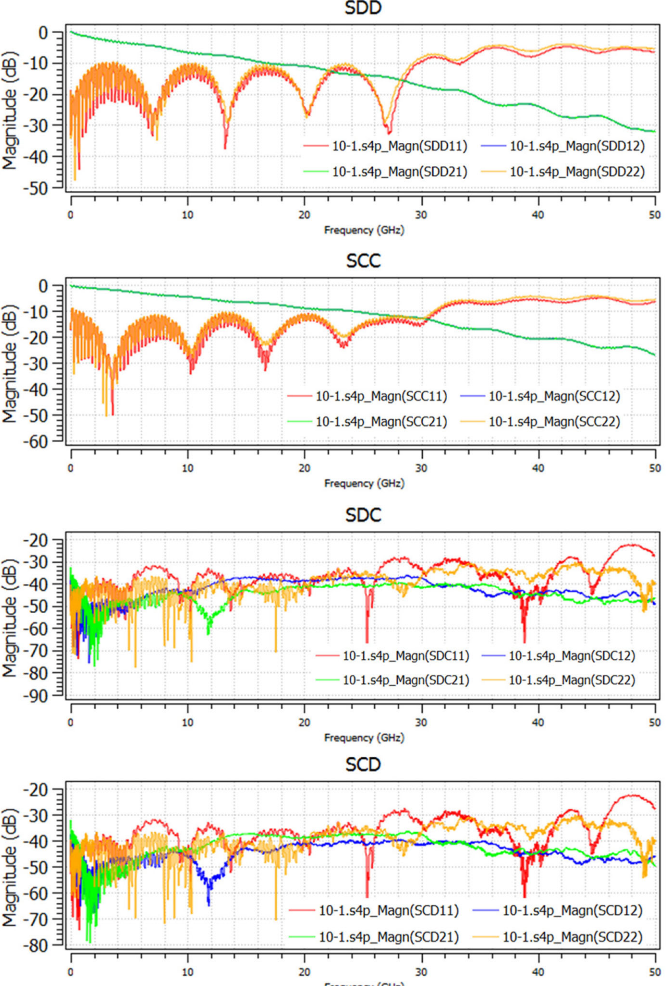

Fig. 2. Mixed-mode *S*-parameters of the 10-in stripline.

complex plane due to the fixture uncertainties [16, Fig. 6]. Based on this assumption, the variation of de-embedded S_{21} can be calculated analytically. However, such "circle" assumption for S_{11} behavior overestimates its variations, since according to the numerical simulation performed by the authors, the spread of S_{11} (at least in certain cases) resembles an ellipse or a crescent rather than a circle.

In this article, a new approach is proposed to analyze the error of de-embedded insertion loss for practical measurements on PCBs. The differences among the fixtures are modeled using the circuits with perturbations determined by the time-domain reflectometry (TDR) measurements. This article is an expanded version of the work published earlier [17], which assumed that the de-embedded transmission coefficient magnitude has a Gaussian distribution. In this article, this assumption is not used and the confidence intervals are estimated more accurately. By using the proposed methodology, engineers can predict the envelope and confidence intervals of the de-embedded insertion loss for a given PCB using just a limited number of simulations. The estimations can be used further to predict the accuracy of the PCB material parameter extraction or to optimize the PCB design to improve the measurement accuracy.

In this article, the method was applied to the differential transmission coefficient, since it is the most important factor limiting the data transmission speed on the high-speed PCBs [18]. Creating models for the single-ended or common-mode transmission coefficients was outside of the scope of this article; however, a similar methodology could be applied to those parameters as well.

This article is organized as follows. In Section II, the model of the fixtures is constructed for the 2X-thru de-embedding method. Section III introduces the error analysis method. The prediction of the envelope of the de-embedding result and the criteria for the estimation of the 99%, 95%, and 90% confidence intervals are provided. The conclusions are given in Section IV.

II. Fixture Modeling

Fig. 1demonstrates a PCB containing a number of striplines that was used as a test vehicle. Two differential pairs with different lengths are selected as the thru and total standards. The 2X-thru de-embedding method is used to illustrate the proposed error analysis approach.

To characterize the four-port transmission lines, the *S*-parameters' measurements using the Keysight N5245A vector network analyzer (VNA) are performed. The working frequency range of the VNA is from 10 MHz to 50 GHz. Prior to the measurements, the VNA is calibrated and the reference planes are set at the ends of the VNA coaxial cables. The four-port nodal (or single-ended) *S*-parameters of the transmission lines are measured and converted to modal ones to produce mixed-mode or common/differential *S*-parameters [18], [19] to directly observe the transmission of the common and differential modes. Due to the symmetry of the lines, the modal conversion is small (as shown in Fig. 2, the conversion terms do not exceed –20 dB), and due to this, the de-embedding techniques are applied to the differential part of the modal scattering matrix as if it represents a single-ended line. However, at high frequencies, the conversion terms become comparable or even larger than the differential transmission coefficient, contributing to de-embedding errors.

Authorized licensed use limited to: Missouri University of Science and Technology. Downloaded on February 01,2021 at 01:15:11 UTC from IEEE Xplore. Restrictions apply.

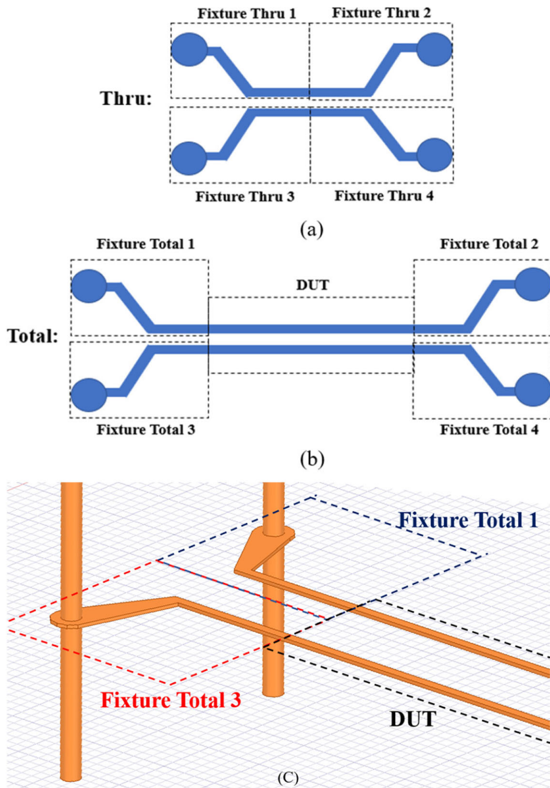

Fig. 3. (a) Thru and (b) total fixture definition. (c) Fixtures and DUT on the total line. The trace width of the differential pairs is 6.58 mil. The spacing between the traces is 5.3 mil. The thickness of the trace is 1.23 mil. The transition length is 340 mil.

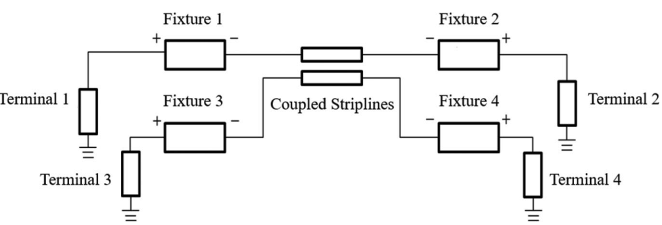

Fig. 4. Overview of the circuit model of the transmission lines with fixtures.

Both thru and total lines include unwanted test fixtures. As Fig. 3 illustrates, the fixtures are composed of the connectors, pads, vias, and transition sections. Many factors will cause the differences between the eight fixtures involved in the calibration process, such as geometrical variations of the PCB layout, slight mechanical displacement of the connectors relative to the PCB layout, nonequal length of the back-drilled stubs in vias connecting surface pads to the inner layer traces [20], and nonidentical torque applied when tightening the connector nuts.

The de-embedding error is obtained by creating statistical models for fixtures. A circuit model of the transmission lines with fixtures was created, as shown in Figs. 4 and 5, following a lumped/distributed modeling approach of the article presented in [21]. Each fixture is modeled by excessive inductance L and capacitance C along with the small portions of matched (to the nominal impedance of 50 Ω) transmission lines (TL1, TL2, TL3)

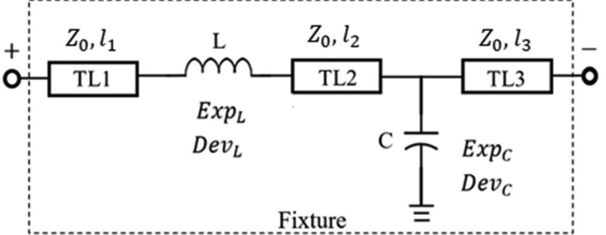

Fig. 5. Fixture circuit model (fixtures 1–4).

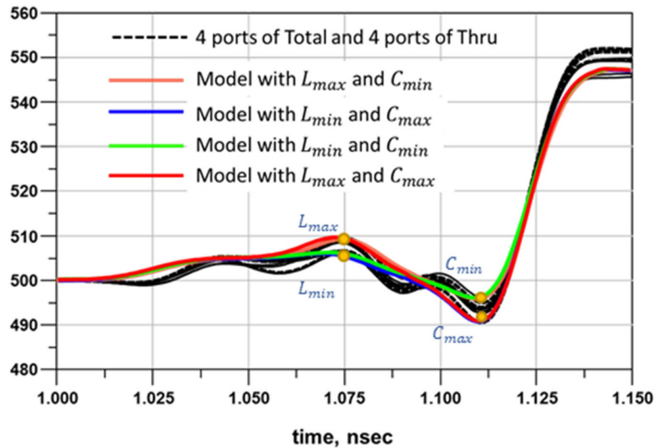

Fig. 6. Measured and modeled fixture TDR responses. The black lines represent the measured curves for eight fixtures. The colored line represents the modeled curves with minimum and maximum excessive L and C values.

added to account for the physical distance between the excessive inductance/capacitance regions.

After the S-parameters are measured, the reflection coefficients are converted to the time domain, and the TDR responses of the fixtures are calculated (see Fig. 6) using a transient solver in the advanced design system [22].

The values of the excessive inductance L and the excessive capacitance C in the fixture model are turned to match the extreme values of the measurement results, as illustrated in Fig. 6. Since two differential lines are used for each measurement, a total of eight TDR curves are available to estimate the spread of the parameters of the fixture models for the thru/total pair. The dielectric constant and attenuation of the coupled stripline in the model in Fig. 4 are tuned to match the de-embedded transmission coefficient in Fig. 2. For the example in Fig. 6, the excessive capacitance is estimated to range from 40.32 to 52.8 fF; the excessive inductance is estimated to range from 1.75 to 17.5 pH. Since the positions of the excessive reactances practically do not change from fixture to fixture (as black curves in Fig. 6 demonstrate), the length of the transmission lines TL1, TL2, and TL3 in the fixture model are kept constant for all fixtures.

Authorized licensed use limited to: Missouri University of Science and Technology. Downloaded on February 01,2021 at 01:15:11 UTC from IEEE Xplore. Restrictions apply.

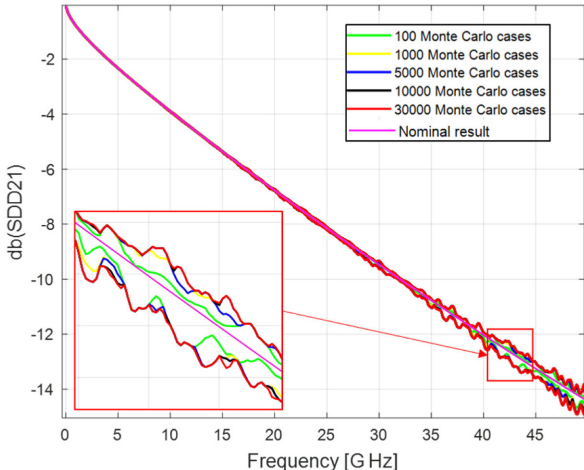

Fig. 7. S_{dd21} envelopes obtained by the Monte–Carlo simulations.

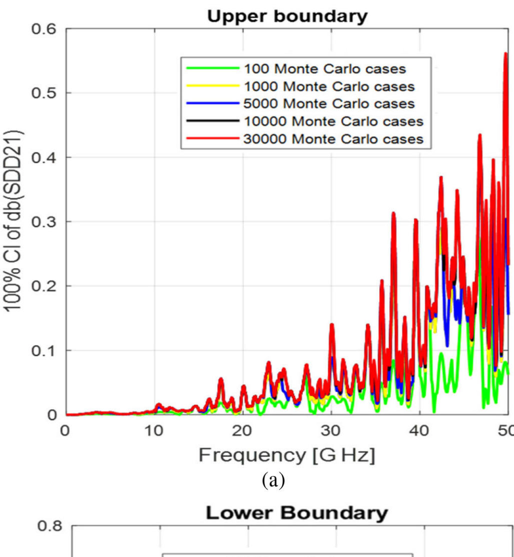

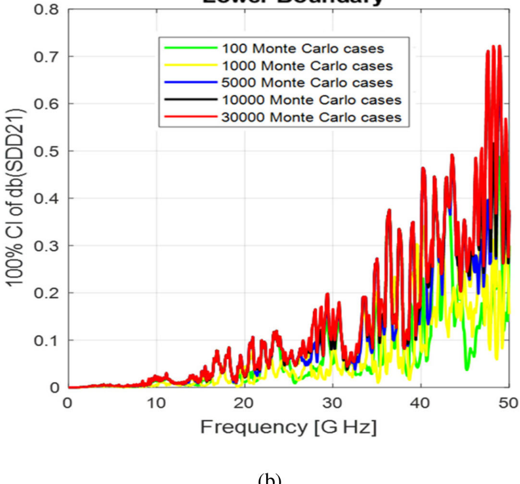

(b)

Fig. 8. 100% confidence interval obtained by the Monte–Carlo simulations. (a) Upper boundary. (b) Lower boundary.

III. Error Analysis

A. Envelope Calculation

To imitate the error caused by the fixture, the perturbations of inductances and capacitances can be added to the fixture model. Since the values of the excessive reactances are bounded, the raw *S*-parameters of the whole circuit model are bounded too. Considering that the singularity caused by the de-embedding procedure is usually avoided in practice, the de-embedded result should also be bounded. The envelope of the de-embedded results (100% confidence interval) represents, therefore, the worst effect of fixtures.

A Monte–Carlo method is commonly applied in stochastic error simulations [23], [24]. A Monte–Carlo simulation of the perturbations for the fixture in the model in Fig. 4 is performed. The excessive reactances are modeled as uniformly distributed random variables with the bounds determined by the TDR responses. For each combination of the random variable values, the *S*-parameters of the lines are calculated using an ac circuit simulator. Finally, the thru/total pairs are created for de-embedding. The envelopes (i.e., the maximum and minimum values at each frequency) of the de-embedded magnitude of the differential transmission coefficient are shown in Fig. 7 along with the nominal curve (no perturbations).

After the Monte–Carlo simulation is performed, it is possible to estimate the relative 100% confidence intervals for the S_{dd21} calculated as

$$\mathrm{CI}_{\mathrm{upper}} = \frac{\max S_{dd21}^{\mathrm{MC}} - S_{dd21}^{\mathrm{nominal}}}{S_{dd21}^{nominal}}$$

$$\mathrm{CI}_{\mathrm{lower}} = \frac{S_{dd21}^{\mathrm{nominal}} - \min S_{dd21}^{\mathrm{MC}}}{S_{dd21}^{\mathrm{nominal}}} \quad (1)$$

where S_{dd21}^{MC} is the set of the values produced by the Monte–Carlo simulation (at each frequency). The corresponding curves are presented in Fig. 8.

As the number of trials in the Monte–Carlo simulations tends to infinity, the confidence intervals (1) will converge to the true 100% probability confidence intervals. As can be seen from the plot, the confidence intervals produced by the Monte–Carlo simulation do converge to a certain value (a difference between the intervals for 10 000 and 30 000 can hardly be noticed).

However, it is extremely difficult to determine the true envelopes using the Monte–Carlo simulation. Indeed, the worst effect is likely to be observed when the differences between the fixtures are the largest, i.e., when the fixture reactances take extreme values. But, since the number of random variables is relatively high (16 reactances for a combination of two lines), the probability of having extreme values in all fixtures is very low.

On the other hand, it is possible to set extreme values to the fixtures directly to calculate the envelopes. Each model in the pair will generate, therefore, 256 cases (two extreme values per eight reactances). The 256 total and 256 thru lines result in 65 536 combinations in total (256^2). The envelopes calculated this way are shown in Figs. 9 and 10 in comparison with the results of the Monte–Carlo simulation. As can be seen, the actual 100% confidence intervals are significantly wider than the ones predicted by the Monte–Carlo simulation.

Authorized licensed use limited to: Missouri University of Science and Technology. Downloaded on February 01,2021 at 01:15:11 UTC from IEEE Xplore. Restrictions apply.

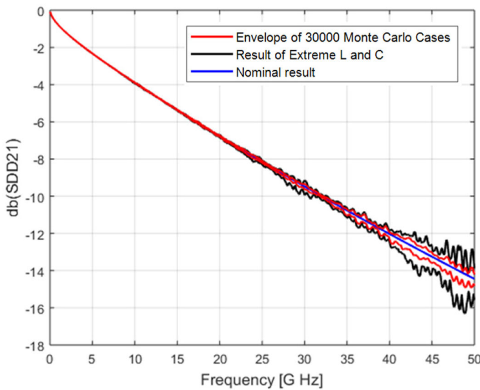

Fig. 9. S_{dd21} envelopes calculated by using the Monte–Carlo simulation and by assigning extreme values to the fixture reactances.

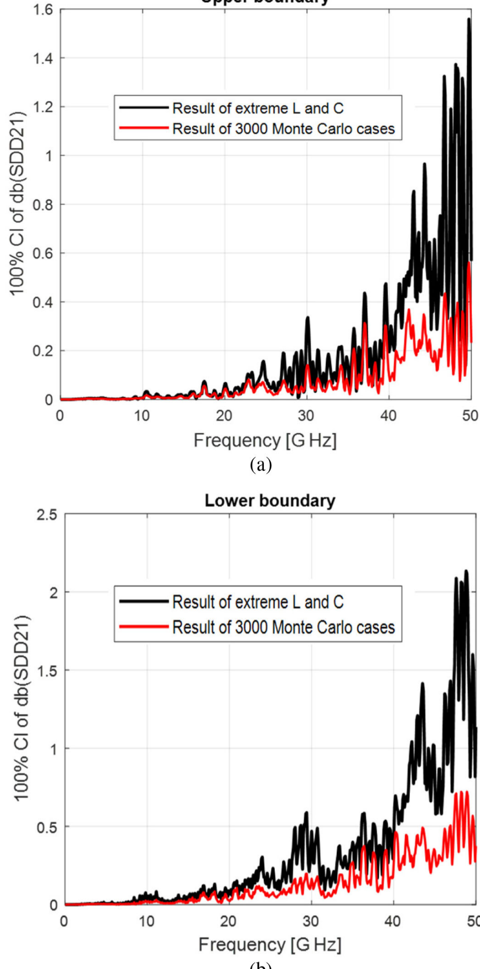

Fig. 10. 100% confidence intervals calculated using the Monte–Carlo simulation and the extreme values of reactances. (a) Upper boundary. (b) Lower boundary.

It is possible to reduce the number of simulations needed to predict the envelopes further. First of all, all symmetrical cases can be excluded (i.e., when fixture 1 is equal to fixture 2, fixture 1 is equal to fixture 3, etc., but not the cases when fixture 1 is equal to fixture 4). This will result in only 4 cases for each line, as shown in Fig. 11, giving 16 cases in total (for all possible pairs of lines). Out of the 16 cases, 6 equivalent cases can be excluded (for example, combinations a–c and b–d are identical with respect to mirroring), leaving just 10 cases, as summarized in Table I.

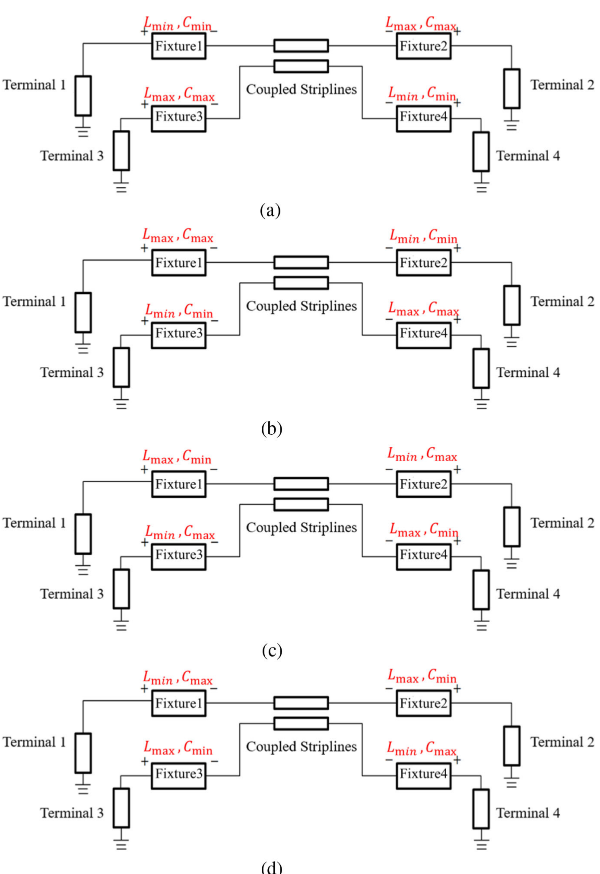

Fig. 11. Four extreme fixture reactance cases used for the envelope prediction. (a) Case a. (b) Case b. (c) Case c. (d) Case d.

TABLE I
TEN CASES FOR THE ENVELOPE PREDICTION

	1	2	3	4	5	6	7	8	9	10
Thru	Case a	Case a	Case a	Case a	Case b	Case c	Case c	Case c	Case c	Case d
Total	Case a	Case b	Case c	Case d	Case a	Case a	Case b	Case c	Case d	Case c

Fig. 12 demonstrates that the envelopes calculated by using 10 remaining cases are the same as the ones obtained by the exhaustive simulation with 65 536 extreme cases.

B. Confidence Interval Estimation

The 100% confidence intervals determined in Section III-A give important insight into the accuracy of the de-embedding. However, as demonstrated earlier, the probability of the worst cases is very low, and the confidence intervals corresponding to the reduced probability might be of larger practical interest.

The reduced probability confidence intervals can be calculated using linear sweeps. Due to the large number of variables, the sweeps cannot be done exhaustively. For example, 8 random

Authorized licensed use limited to: Missouri University of Science and Technology. Downloaded on February 01,2021 at 01:15:11 UTC from IEEE Xplore. Restrictions apply.

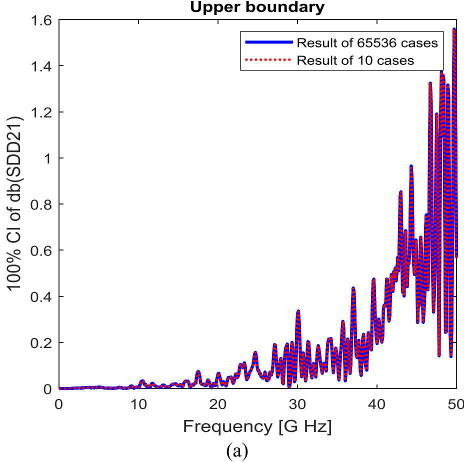

(a)

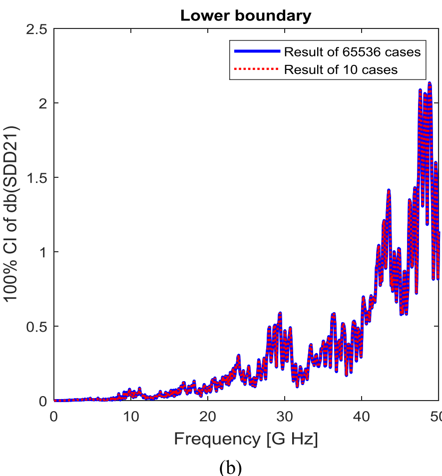

(b)

Fig. 12. 100% confidence interval of exhaustive simulation with 65 536 extreme reactance cases and 10 selected cases. (a) Upper boundary. (b) Lower boundary.

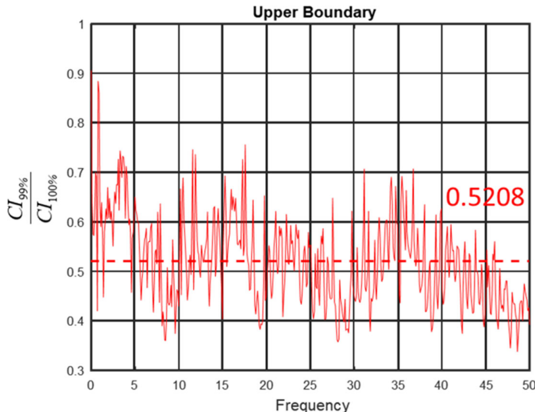

Fig. 13. Ratio of 99% confidence interval to 100% confidence interval for the upper boundary.

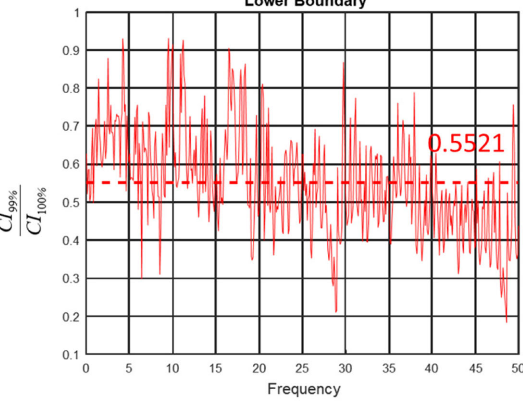

Fig. 14. Ratio of 99% confidence interval to 100% confidence interval for the lower boundary.

variables with just 5 values within the bounds would produce 32 768 cases for each line, resulting in 1 073 741 824 possible thru/total combinations. However, similarly to the estimation of the envelopes, the number of combinations can be reduced by excluding the symmetrical cases. This leaves only 4 cases for each transmission line, resulting in just 390 625 cases for 5 values within the bounds $(5^4 \cdot 5^4)$, which can be practically implemented to estimate the confidence intervals.

On the other hand, exhaustive sweep with the large number of variables might be difficult to implement in typical engineering practice, and the simulation can be time-consuming. As an alternative, we propose a confidence interval estimation method that is based on scaling the envelopes (100% confidence intervals).

Suppose the confidence intervals are determined by the linear sweep, then it is possible to calculate the ratio of the boundaries of the envelopes to the boundaries of the confidence intervals. The examples of such calculations are presented in Figs. 13 and 14. As can be seen, the ratios are frequency dependent. However, their spread is relatively small. Approximately each ratio can be represented by its mean value (dashed curves in the figures). After this is done, the confidence interval for probability p (lower or upper boundary) can be estimated as

$$\mathrm{CI}_p^{\mathrm{est}} \approx \frac{\mathrm{CI}_p}{\mathrm{CI}_{100\%}} \mathrm{CI}_{100\%} \tag{2}$$

where $\langle\cdot\rangle$ represents averaging over the frequency range, $\mathrm{CI}_{100\%}$ is the envelope, and CI_p is the actual confidence interval for the probability p calculated by linearly sweeping the parameters (in the cases presented next, 5 values were taken within the bounds for each parameter; for each transmission line, 4 parameters were swept, resulting in 625 (5^4) cases and 390 625 combinations in total).

Of course, using the mean ratio instead of the actual frequency-dependent value introduces the additional errors, but they are relatively low in the entire frequency range on average. For example, the root-mean-square error between the average and the actual curve for Fig. 13 is 15% and for Fig. 14 is 18%.

Approach (1) could be useful only if the mean ratio depends on the probability level only and does not depend (or at least depends weakly) on the fixtures, transmission line parameters (length, attenuation), etc. In other words, the probability distribution of the attenuation curve is invariant.

To investigate that, a series of simulations were performed with the model parameters. To achieve this, all available transmission lines PCB in Fig. 1 were used as thru [resulting in

Authorized licensed use limited to: Missouri University of Science and Technology. Downloaded on February 01,2021 at 01:15:11 UTC from IEEE Xplore. Restrictions apply.

TABLE II
CI TO ENVELOPE MEAN RATIO FOR DIFFERENT DUT LENGTHS

	DUT length	Upper	Lower
$\frac{CI_{99\%}}{CI_{100\%}}$	4.5 inch	0.5107	0.5292
	5.0 inch	0.5034	0.5260
	9.5 inch	0.5028	0.5347
$\frac{CI_{95\%}}{CI_{100\%}}$	4.5 inch	0.3460	0.3461
	5.0 inch	0.3385	0.3458
	9.5 inch	0.3654	0.3516
$\frac{CI_{90\%}}{CI_{100\%}}$	4.5 inch	0.2634	0.2536
	5.0 inch	0.2562	0.2524
	9.5 inch	0.2684	0.2685

Fixture delay=0.025 ps, fixture reactances: $C \in [40.32\,\text{fF}; 52.8\,\text{fF}]$; $L \in [1.75\,\text{pH}; 17.5\,\text{pH}]$.

TABLE III
CI TO ENVELOPE MEAN RATIO FOR DIFFERENT FIXTURE DELAYS

	Fixture Delay	Upper	Lower
$\frac{CI_{99\%}}{CI_{100\%}}$	0.0125 ps	0.5240	0.5314
	0.025 ps	0.5107	0.5292
	0.050 ps	0.5172	0.5304
$\frac{CI_{95\%}}{CI_{100\%}}$	0.0125 ps	0.3207	0.3663
	0.025 ps	0.3460	0.3461
	0.050 ps	0.3395	0.3462
$\frac{CI_{90\%}}{CI_{100\%}}$	0.0125 ps	0.2462	0.2734
	0.025 ps	0.2634	0.2536
	0.050 ps	0.2571	0.2535

DUT length=9.5 in, fixture reactances: $C \in [40.32\text{ fF}; 52.8\text{ fF}]$; $L \in [1.75\text{ pH}; 17.5\text{ pH}]$.

TABLE IV
CI TO ENVELOPE MEAN RATIO FOR DIFFERENT FIXTURE REACTANCE BOUNDS

	Fixture reactance	Upper	Lower
$\frac{CI_{99\%}}{CI_{100\%}}$	$C \in [40.32\text{ fF}; 52.8\text{ fF}]$ $L \in [1.75\text{ pH}; 17.5\text{ pH}]$	0.5107	0.5292
	$C \in [80.64\text{ fF}; 105.6\text{ fF}]$ $L \in [3.5\text{ pH}; 35\text{ pH}]$	0.4931	0.5427
	$C \in [20.16\text{ fF}; 26.4\text{ fF}]$ $L \in [0.875\text{ pH}; 8.75\text{ pH}]$	0.4826	0.5144
$\frac{CI_{95\%}}{CI_{100\%}}$	$C \in [40.32\text{ fF}; 52.8\text{ fF}]$ $L \in [1.75\text{ pH}; 17.5\text{ pH}]$	0.3460	0.3461
	$C \in [80.64\text{ fF}; 105.6\text{ fF}]$ $L \in [3.5\text{ pH}; 35\text{ pH}]$	0.3485	0.3674
	$C \in [20.16\text{ fF}; 26.4\text{ fF}]$ $L \in [0.875\text{ pH}; 8.75\text{ pH}]$	0.3137	0.3709
$\frac{CI_{90\%}}{CI_{100\%}}$	$C \in [40.32\text{ fF}; 52.8\text{ fF}]$ $L \in [1.75\text{ pH}; 17.5\text{ pH}]$	0.2634	0.2536
	$C \in [80.64\text{ fF}; 105.6\text{ fF}]$ $L \in [3.5\text{ pH}; 35\text{ pH}]$	0.2394	0.2543
	$C \in [20.16\text{ fF}; 26.4\text{ fF}]$ $L \in [0.875\text{ pH}; 8.75\text{ pH}]$	0.2399	0.2785

DUT length=9.5 in, fixture delay=0.025 ps.

device under tests with the equivalent lengths of 4.5 in (5.8-1.3), 5.0 in (10.8-5.8), and 9.5 in (10.8-1.3)]. The fixture delay and fixture reactances were scaled up and down by two resulting in additional cases. The ratios for 99%, 95%, and 90% confidence intervals were calculated for the original and modified cases. The results are summarized in the following tables:

1) three DUT length (see Table II);
2) three fixture delay (see Table III);
3) two scaled fixture reactance bounds (see Table IV).

As can be seen, the ratios $\frac{\text{CI}_p}{\text{CI}_{100\%}}$ remain relatively constant and are close to 0.5 for 99% probability, 0.35 for 95% probability, and 0.25 for 90% probability.

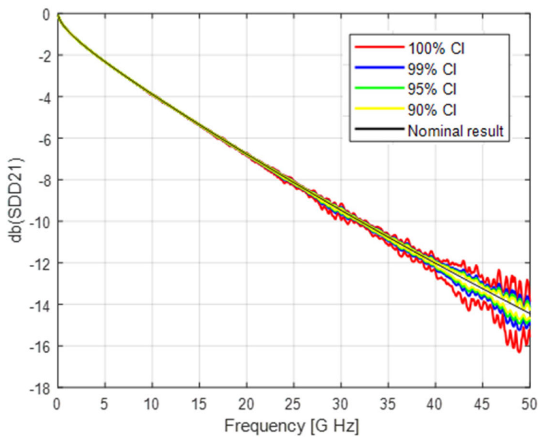

Fig. 15. Estimated S_{dd21} confidence intervals for different probability levels.

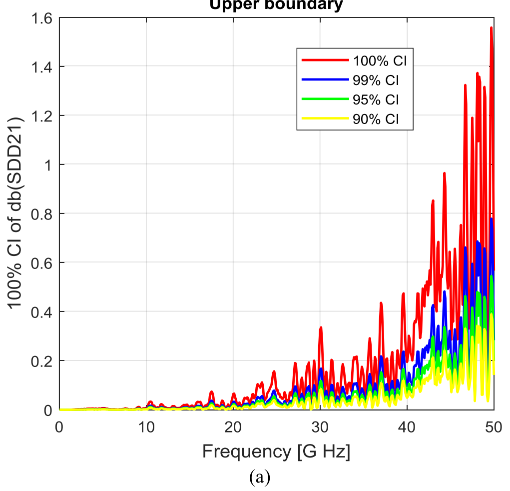

(a)

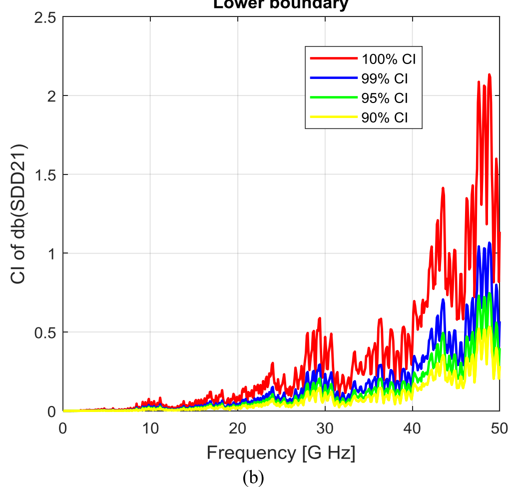

(b)

Fig. 16. Confidence interval estimation for the upper and lower boundary.

Authorized licensed use limited to: Missouri University of Science and Technology. Downloaded on February 01,2021 at 01:15:11 UTC from IEEE Xplore. Restrictions apply.

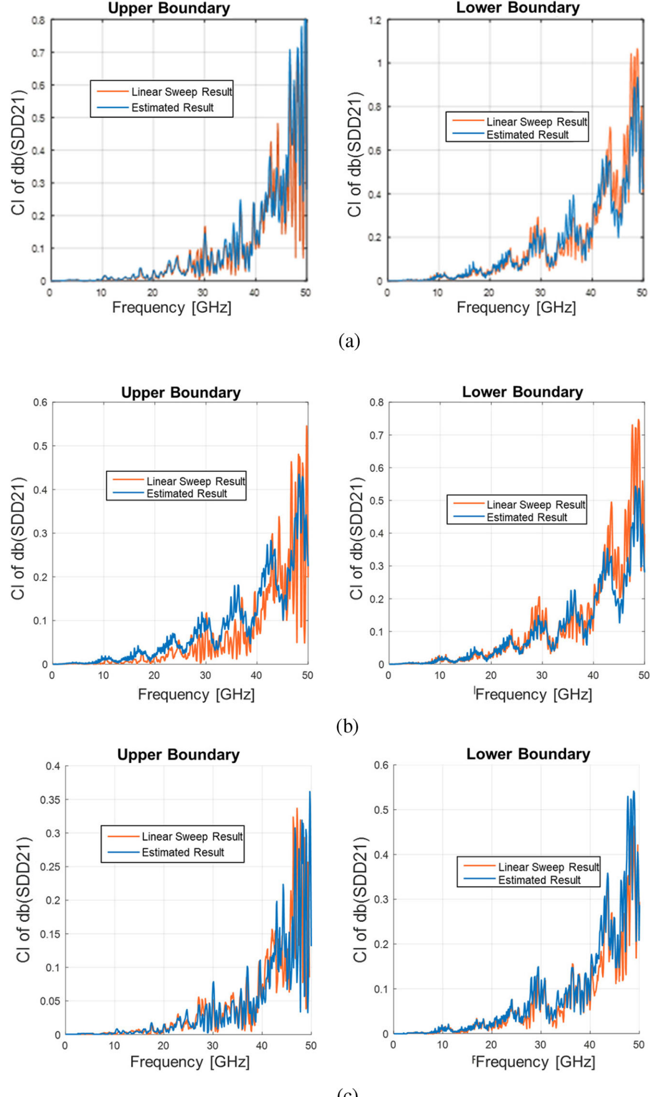

Fig. 17. Comparison between the estimated confidence intervals and confidence interval determined by the linear sweep. (a) 99% confidence interval. (b) 95% confidence interval. (c) 90% confidence interval.

The estimated confidence intervals calculated according to (2) using the mean ratios of 0.5, 0.35, and 0.25 for 99%, 95%, and 90% probabilities correspondingly are shown in Figs. 15 and 16.

Finally, Fig. 17 shows a comparison between the confidence intervals estimated by (2) and determined by the linear sweep of the fixture parameters, demonstrating practically acceptable agreement.

IV. Conclusion

This article presents a methodology to perform error estimation for de-embedding methods. Unlike other de-embedding sensitivity investigations, it is proposed for practical PCB measurement. The differences among fixtures are modeled using circuits with extreme values determined by TDR measurement. The envelope of the insertion loss variance can be predicted using just ten simulation cases. The 99%, 95%, and 90% confidence intervals are estimated by scaling the envelopes with the corresponding mean ratios.

The proposed methodology can be used to estimate the achievable accuracy of the existing measurement fixtures or to optimize the fixture design (requited fixture reactances and their spread, optimal thru/total pair, etc.) in order to meet a certain de-embedding accuracy target.

References

[1] Keysight Technol., "The ABCs of de-embedding." [Online]. Available: http://literature.cdn.keysight.com/ litweb/pdf/5989-5765EN.pdf, Accessed on: Dec. 2018.

[2] G. F. Engen and C. A. Hoer, "Thru-reflect-line: An improved technique for calibrating the dual six-port automatic network analyzer," *IEEE Trans. Microw. Theory Techn.*, vol. 27, no. 12, pp. 987–993, Dec. 1979.

[3] B. Chen, X. Ye, B. Samaras, and J. Fan, "A novel de-embedding method suitable for transmission-line measurement," in *Proc. Asia-Pac. Symp. Electromagn. Compat.*, Taipei, Taiwan, 2015, pp. 1–4.

[4] Q. Huang, J. Li, J. Zhou, W. Wu, Y. Qi, and J. Fan, "De-embedding method to accurately measure high-frequency impedance of an O-shape spring contact," in *Proc. IEEE Int. Symp. Electromagn. Compat.*, Raleigh, NC, USA, 2014, pp. 600–603.

[5] Y. Chen, B. Chen, J. He, R. Zai, J. Fan, and J. Drewniak, "De-embedding comparisons of 1X-reflect SFD, 1-port AFR, and 2X-thru SFD," in *Proc. IEEE Asia-Pac. Symp. Electromagn. Compat.*, Singapore, May 14–18, 2018, pp. 160–164.

[6] B. Chen *et al.*, "Differential S-parameter de-embedding for 8-port network," in *Proc. IEEE Symp. Electromagn. Compat., Signal Integrity Power Integrity*, Long Beach, CA, USA, Aug. 2018, pp. 52–56.

[7] S. Yong, V. Khilkevich, X.-D. Cai, C. Sui, B. Sen, and J. Fan, "Comprehensive and practical way to look at far-end crosstalk for transmission lines with lossy conductor and dielectric," *IEEE Trans. Electromagn. Compat.*, vol. 62, no. 2, pp. 510–520, Apr. 2020.

[8] B. Chen *et al.*, "Differential integrated crosstalk noise (ICN) reduction among multiple differential BGA and via pairs by using design of experiments (DoE) method," in *Proc. IEEE Int. Symp. Electromagn. Compat. Signal/Power Integrity*, Washington, DC, USA, Aug. 7–11, 2017, pp. 112–117.

[9] S. Yong, K. Cai, B. Sen, J. Fan, V. Khilkevich, and C. Sui, "A comprehensive and practical way to look at crosstalk for transmission lines with mismatched terminals," in *Proc. IEEE Int. Symp. Electromagn. Compat., Signal Integrity Power Integrity*, Long Beach, CA, USA, Jul. 30–Aug. 3, 2018, pp. 538–543.

[10] X. Guo *et al.*, "Design methodology for behavioral surface roughness model," in *Proc. IEEE Int. Symp. Electromagn. Compat.*, Ottawa, ON, Canada, 2016, pp. 927–931.

[11] S. Jin, X. Fang, B. Chen, H. Gao, X. Ye, and J. Fan, "Validating the transmission-line based material property extraction procedure including surface roughness for multilayer PCBs using simulations," in *Proc. IEEE Int. Symp. Electromagn. Compat.*, Ottawa, ON, Canada, Jul. 2016, pp. 472–477.

[12] S. Yong *et al.*, "Dielectric dissipation factor (DF) extraction based on differential measurements and 2-D cross-sectional analysis," in *Proc. IEEE Int. Symp. Electromagn. Compat., Signal Integrity Power Integrity*, Long Beach, CA, USA, Jul. 30–Aug. 3, 2018, pp. 217–222.

[13] B. Chen *et al.*, "Analytical and numerical sensitivity analyses of fixtures de-embedding," in *Proc. IEEE Int. Symp. Electromagn. Compat.*, 2016, pp. 440–444.

[14] G. Yin, X.-D. Cai, D. Secker, M. Ortiz, J. Cline, and A. Vaidyanath, "Impedance perturbation theory for coupled uniform transmission lines," *IEEE Trans. Electromagn. Compat.*, vol. 57, no. 2, pp. 299–308, Apr. 2015.

[15] L. Ye *et al.*, "Thru-reflect-line calibration technique: Error analysis for characteristic impedance variations in the line standards," *IEEE Trans. Electromagn. Compat.*, vol. 59, no. 2, pp. 779–788, Jun. 2017.

[16] C. Wu, B. Chen, T. Mikheil, J. Fan, and X. Ye, "Error bounds analysis of de-embedded results in 2x thru de-embedding methods," in *Proc. IEEE Int. Symp. Electromagn. Compat. Signal/Power Integrity*, Washington, DC, USA, Aug. 2017, pp. 532–536.

Authorized licensed use limited to: Missouri University of Science and Technology. Downloaded on February 01,2021 at 01:15:11 UTC from IEEE Xplore. Restrictions apply.

[17] S. Yonget al., "A practical de-embedding error analysis method based on statistical circuit models of fixtures," in *Proc. IEEE Int. Symp. Electromagn. Compat., Signal Power Integrity*, New Orleans, LA, USA, 2019, pp. 45–50.
[18] E. Bogatin, *Signal and Power Integrity—Simplified*, 2nd ed. London, U.K.: Pearson Educ., 2009, ch. 12.
[19] S. Yonget al., "Dielectric loss tangent extraction using modal measurements and 2-D cross-sectional analysis for multilayer PCBs," *IEEE Trans. Electromagn. Compat.*, to be published, doi: 10.1109/TEMC.2019.2949021.
[20] H. Gao, S. De, B. Beingessner, S. Payne, and J. Drewniak, "Misregistration of sliver type backdrill impact in high speed signal propagation," in *Proc. IEEE Symp. Electromagn. Compat., Signal Integrity Power Integrity*, Long Beach, CA, USA, Aug. 2018, pp. 62–65,
[21] J. M. Jong, V. K. Tripathi, and B. Janko, "Equivalent circuit modeling of interconnects from time domain measurements," in *Proc. 42nd Electron. Compon. Technol. Conf.*, 1992, pp. 730–735.
[22] Keysight Technol., "Transient and convolution simulation." [Online]. Available: http://edadownload. software.keysight.com/eedl/ads/2011/pdf/cktsimtrans.pdf, Accessed on: Mar. 2020.
[23] J. P. Hoffmann, P. Leuchtmann, J. Schaub, and R. Vahldieck, "Computing uncertainties of S-parameters by means of Monte Carlo simulation," in *Proc. 69th ARFTG Conf.*, Honolulu, HI, USA, 2007, pp. 1–7.
[24] J. Lee, Y. Lee, and H. Kim, "Decision of error tolerance in array element by the Monte Carlo method," *IEEE Trans. Antennas Propag.*, vol. 53, no. 4, pp. 1325–1331, Apr. 2005.

Yuanzhuo Liu (Student Member, IEEE) received the B.E. degree in electrical and computer engineering from the Huazhong University of Science and Technology, Wuhan, China, in 2017, and the M.S. degree in electrical engineering, in 2019 from the Missouri University of Science and Technology (formerly University of Missouri - Rolla), Rolla, MO, USA, where she is currently working toward the Ph.D. degree in electrical engineering with Electromagnetic Compatibility Laboratory.

Her research interests include electromagnetic interference, signal integrity in high-speed digital systems, and microwave imaging.

Shaohui Yong (Student Member, IEEE) received the B.S. degree in electrical engineering from Beijing Jiaotong University, Beijing, China, in 2013, and the M.S. degree in electrical engineering, in 2015 from the Missouri University of Science and Technology (formerly University of Missouri - Rolla), Rolla, MO, USA, where he is currently working toward the Ph.D. degree in electrical engineering with Electromagnetic Compatibility Laboratory.

His research interests focus on signal integrity in high-speed digital systems, electromagnetic simulation, and measurement techniques.

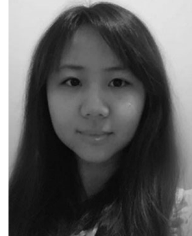

Han Gao (Student Member, IEEE) received the M.S. degree in electrical engineering from Electromagnetic Compatibility Laboratory, Missouri University of Science and Technology (University of Missouri–Rolla), Rolla, MO, USA, in 2019.

She is currently a Signal Integrity Engineer with Cisco Systems, Inc., San Jose, CA, USA. Her research interests include surface roughness modeling in the printed circuit board (PCB), SerDes characterization, power integrity in both ASIC and PCB level, and generic differential transmission line modeling.

Scott Hinaga received the B.S. degree in chemistry from Stanford University, Stanford, CA, USA, in 1985.

He has been with Cisco Systems, Inc., San Jose, CA, USA, for ten years, with 20 years of prior experience in the printed circuit board (PCB) manufacturing engineering management. He is a Staff Manufacturing Engineer with the PCB Technology Group. His main projects have involved research and qualification of high-speed/low-loss PCB laminates, foil, and glass, as well as the characterization of conductor surface roughness effects on insertion loss.

Darja Padilla received the Ph.D. degree in electrical engineering from the University of Colorado Boulder, Boulder, CO, USA, with a concentration in optics and electromagnetics.

She is currently a Technical Leader with Cisco Systems, Inc., San Jose, CA, USA. Her main projects involve high-speed board and ASIC package design, and advanced material characterization.

Douglas Yanagawa received the M.S. degree in electrical engineering from Santa Clara University, Santa Clara, CA, USA, in 1990.

He was a Microprocessor Package Designer with MIPS Computer Systems, Inc., and a Signal Integrity Engineer with Silicon Graphics, Inc. Since 1998, he has been a Signal Integrity Engineer with Cisco Systems, Inc., San Jose, CA, USA.

James L. Drewniak (Fellow, IEEE) received the B.S., M.S., and Ph.D. degrees in electrical engineering from the University of Illinois at Urbana–Champaign, Champaign, IL, USA, in 1985, 1987, and 1991, respectively.

He is currently with Electromagnetic Compatibility Laboratory, Department of Electrical and Computer Engineering, Missouri University of Science and Technology, Rolla, MO, USA. His research interests include electromagnetic compatibility, signal and power integrity, and electronic packaging.

Victor Khilkevich (Member, IEEE) received the Ph.D. degree in electrical engineering from Moscow Power Engineering Institute, Technical University, Moscow, Russia, in 2001.

He is currently an Associate Research Professor with the Missouri University of Science and Technology, Rolla, MO, USA. His research interests include microwave imaging, automotive electromagnetic compatibility modeling, and high-frequency measurement techniques.

Authorized licensed use limited to: Missouri University of Science and Technology. Downloaded on February 01,2021 at 01:15:11 UTC from IEEE Xplore. Restrictions apply.